ACS APPLIED MATERIALS & INTERFACES

Research Article

www.acsami.org

Ultrasonically Assisted Polysaccharide Microcontainers for Delivery of Lipophilic Antitumor Drugs: Preparation and in Vitro Evaluation

Roman Akasov,[*,†,‡] Tatiana Borodina,[‡] Ekaterina Zaytseva,[†] Anastasia Sumina,[†] Tatiana Bukreeva,[‡,§] Sergey Burov,[∥] and Elena Markvicheva[†]

[†]Polymers for Biology Laboratory, Shemyakin-Ovchinnikov Institute of Bioorganic Chemistry of the Russian Academy of Sciences, 117997, Miklukho-Maklaya 16/10, Moscow, Russia

[‡]Laboratory of Bioorganic Structures, Shubnikov Institute of Crystallography of the Russian Academy of Sciences, 119333, Leninskii Prospekt 59, Moscow, Russia

[§]National Research Centre, Kurchatov Institute, 123182, Akademika Kurchatova Ploshchad 1, Moscow, Russia

[∥]Synthesis of Peptides and Polymer Microspheres Laboratory, Institute of Macromolecular Compounds of the Russian Academy of Sciences, 199004, Bolshoy Prospekt 31, Saint-Petersburg, Russia

ABSTRACT: High toxicity, poor selectivity, and severe side effects are major drawbacks of anticancer drugs. Various drug delivery systems could be proposed to overcome these limitations. The aim of this study was to fabricate polysaccharide microcontainers (MCs) loaded with thymoquinone (TQ) by a one-step ultrasonication technique and to study their cellular uptake and cytotoxicity in vitro. Two MC fractions with a mean size of 500 nm (MC-0.5) and 2 μM (MC-2) were prepared and characterized. Uptake of the MCs by mouse melanoma M-3 cells was evaluated in both 2D (monolayer culture) and 3D (multicellular tumor spheroids) models by confocal microscopy, flow cytometry, and fluorimetry. The higher cytotoxicity of the TQ-MC-0.5 sample than the TQ-MC-2 fraction was in good correlation with higher MC-0.5 accumulation in the cells. The MC-0.5 beads were more promising than the MC-2 particles because of a higher cellular uptake in both 2D and 3D models, an enhanced antitumor effect, and a lower nonspecific toxicity.

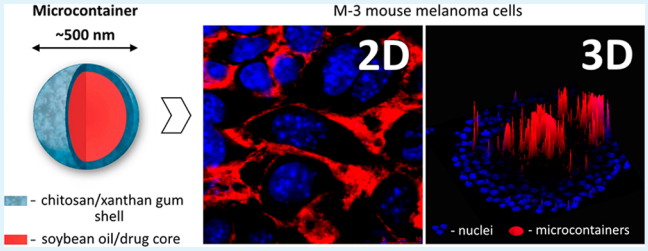

KEYWORDS: *drug delivery systems, chitosan, xanthan gum, multicellular tumor spheroids, ultrasonication, microcontainers*

1. INTRODUCTION

As well-known, most of anticancer drugs used in clinics suffer from poor drug solubility in water and low selectivity and bioavailability. Usage of surfactants in drug formulations allows one to improve drug solubility but may lead to severe side effects. Thus, the docetaxel-based formulation Taxotere contains a rather high amount of Tween 80 (40 g/L), which provokes hypersensitivity, possible hemolysis, and cumulative fluid retention.[1] The paclitaxel-based formulation Taxol contains Cremophor EL, which can induce hypersensitivity reactions, reducing paclitaxel uptake and, as a result, decreasing drug efficacy.[2] Presently, numerous research groups are focused on design of new anticancer drug delivery systems, in order to reduce these side effects, improve drug solubility, and provide targeted drug delivery as well as sustained/controlled drug release.

There are a lot of techniques commonly used for preparation of various drug delivery systems, such as liposomes, polymer-based systems (PCL−PEG, PLGA, PLGA−PEG nanospheres), micelles, micro- and nanoemulsions, nanogels, and solid lipid nanoparticles.[3] Ultrasonication is an alternative promising technique that is based on an acoustic cavitation deriving from the continuous formation, growth, and implosive collapse of bubbles in a liquid.[4] This approach is characterized by the complete avoidance of toxic cross-linking chemicals and emulsifiers, environmentally harmful volatile organic compounds, or metal-based catalysts, which are used in other techniques. Moreover, the ultrasonically induced encapsulation technique is less time and energy consuming, while using rather compact equipment. Ultrasonication was first proposed by Grinstaff and Suslick for preparation of protein microspheres from bovine and human serum albumins.[5] Since this publication, a number of research groups have used this approach to fabricate various ultrasonic-induced particles.[6] It has been claimed that one-step sonochemical encapsulation is extremely promising to produce a core−shell structure with high drug loading.[7] Recently, we developed a new class of microcontainers based on chitosan (CS) and xanthan gum (XG) by a low-frequency ultrasonication.[8] Both polymers belong to natural polysaccharides, which are biocompatible, biodegradable, and widely employed for fabrication of micro-

Received: May 13, 2015
Accepted: July 9, 2015
Published: July 9, 2015

DOI: 10.1021/acsami.5b04141
ACS Appl. Mater. Interfaces 2015, 7, 16581−16589

capsules.[9,10] Additionally, polysaccharides can stabilize the shell of microcontainers (MCs) within a broad pH range.

In this study, chitosan/xanthan gum MCs were proposed for delivery of lipophilic anticancer drug. Although chitosan-based or xanthan-gum-based delivery systems are not approved by FDA for intravenous injection, they could be administrated intratumorally, orally, or transdermally.[11−13] Both of these polymers are widely reported for development of various drug delivery systems, in particular, chitosan nanoparticles for melanoma treatment.[14,15] Natural compounds with antitumor properties are of great interest, since they are rather cheap and nontoxic for normal cells. Thymoquinone (TQ), which was selected here as a model lipophilic drug, is the main active component of black seed essential oil. It was found to possess both anti-inflammatory and anticancer effects due to inhibiting both tumor metastasis and angiogenesis.[16,17] TQ is unstable in aqueous medium, particularly at an alkaline pH, and light sensitive.[18] Encapsulation could not only increases the TQ bioavailability but also protect the drug from degradation caused by external factors, limiting its diffusion to normal tissues and preventing rapid release.[19] The aim of the current study was to fabricate ultrasonically induced polysaccharide microcontainers loaded with thymoquinone and to study cellular uptake and cytotoxicity of the obtained MCs under both 2D (monolayer culture) and 3D (tumor spheroids) conditions.

2. EXPERIMENTAL SECTION

2.1. Materials. Low molecular weight chitosan [20−300 cps, 1 wt % in 1% acetic acid (25 °C), 75−85% deacetylated], xanthan gum [from *Xanthomonas campestris*, 800−1200 cps, 1% in H_2O (25 °C)], soybean oil, Nile Red (NR), thymoquinone (2-isopropyl-5-methyl-1,4-benzoquinone, 99%), Hoechst 33258, MTT (Thiazolyl Blue Tetrazolium Bromide, 98%), poly-L-lysine (PLL) with molecular weight of 40 000−60 000 Da, and DiO fluorescent dye (3,3′-dioctadecyloxacarbocyanine perchlorate, 97%) were from Sigma-Aldrich. DMSO (dimethyl sulfoxide, 99.5%), Trypan Blue solution, phosphate-buffered saline (PBS, pH 7.4), 0.25% (v/v) trypsin-EDTA solution, and Dulbecco's modified Eagle's medium (DMEM) were purchased from PanEko (Moscow, Russia), and fetal bovine serum (FBS) was from PAA. Cyclo-RGDfK(TPP) (MW 1029) was obtained by covalent attachment of triphenylphosphine (TPP) to cyclo-RGDfK peptide, which was synthesized according to standard solid-phase peptide synthesis protocols, as previously described.[53]

2.2. Preparation of the Microcontainers. In the preparation of chitosan solution, chitosan was dissolved at 0.25% w/v in 0.1 M HCl, whereas xanthan gum solution was prepared by dissolving 0.25% (w/v) in deionized water. In both cases, the pH was adjusted to 2 with 0.1 M HCl (the acidic pH of the solutions is prerequisite to avoid electrostatic interaction between the polysaccharides in the mixture). Chitosan/xanthan gum MCs were obtained as described earlier.[8] Briefly, equal volumes (2 mL) of chitosan and xanthan gum solutions (0.25% w/v, pH 2) were mixed, and then soybean oil containing TQ (100 mg/mL) or NR (10 mg/mL) was added, and the mixture was exposed to high-intensity ultrasound using a 7 mm diameter titanium sonotrode (56 $W \cdot cm^{-2}$, 20 kHz, 5 min) (Ultrasonic Processor UP400S, Hielscher Ultrasonics GmbH). An oil/water ratio of 1:150 or 1:30 was used to generate MCs 0.5 and 2 μm in diameter, respectively. The obtained MCs were separated from the reaction mixture by centrifugation (6.708*g*, 5 min) and washed three times with Milli-Q water. The encapsulated TQ content was estimated by determining the difference in drug concentration in the solution before and after MC synthesis using UV−vis spectroscopy at 257 nm (PerkinElmer Lambda 650). The encapsulation efficiency was up to 95%. To modify the MC surface with poly-L-lysine, 100 μL of the MC solution was added to 1 mL of a 0.2% (w/v) PLL solution in 0.15 N NaCl, and the mixture was shaken for 15 min (IKA MS3 basic, IKA Works Inc.). Then, the obtained MCs were separated by centrifugation (6.708*g*, 5 min) and washed with Milli-Q water.

2.3. Characterization of the Microcontainers. An average MC diameter, particle homogeneity (polydispersity index, PI), and a surface charge (ζ-potential) were measured by DLS using a ZetaSizer Nano equipped with a 4 mW He−Ne laser (Malvern Instruments). A mean ζ-potential value was calculated from three subsequent measurements (each was 15 runs), while the mean size of the MCs was determined from five subsequent measurements (each was 20 runs).

2.4. Cryo-Scanning Electron Microscopy. Microcontainer morphology was studied by cryo-scanning electron microscopy (cryo-SEM) according to Borodina et al.[8] Briefly, each sample was frozen by plunging it into a nitrogen slush at atmospheric pressure. Samples were freeze-fractured at −150 °C, etched for 60 s at −98 °C, sputtered with platinum in a GATAN Alto 2500 Cryo preparation chamber, and then transferred into a cryo-SEM system.

2.5. Cell Culture and Formation of Tumor Spheroids. Mouse melanoma M3 cell line (Cloudman S91 melanoma) was used as a model in this study. Cells were cultivated in DMEM supplemented with 10% FBS in a 5% CO_2 humidified atmosphere at 37 °C. The cells were detached after treatment with a 0.25% (v/v) trypsin−EDTA solution, and the medium was replaced every 3−4 days. Multicellular tumor spheroids (MTSs) were obtained as described previously.[53] Briefly, cells (50 000 cells/mL) were seeded in a 96-well plate (100 μL/well) and incubated at 37 °C for 2−3 h until the cells attached to the plate bottom. Then the medium was replaced with 100 μL of full DMEM containing a cyclo-RGDfK(TPP) peptide (40 μM). Finally, the plate was transferred to a CO_2-incubator, and RGD-induced MTS formation was observed in 2−3 days.

2.6. Cytotoxicity Study. Cells were seeded in a 96-well plate (5000 cells/well) followed by overnight incubation. A TQ stock solution was prepared as a 1% (w/v) TQ solution in DMSO, and working dilutions (0.1, 1, 10, 50, 100 μg/mL) were prepared in DMEM (10% FBS) immediately prior to experiments. Aliquots (100 μL) of these TQ dilutions, TQ-loaded MC suspensions (1, 10, 50, 100, 200, 300 μg/mL), or blank MC (1, 2.5, 5, 7.5, 10 μL/mL) were added to each well with the cells, and the plates were transferred to the CO_2-incubator for 24, 48, and 72 h. After treatment, the cells were stained with a 0.05% (w/v) MTT solution in DMEM for 4 h. Then, to dissolve formed formazan crystals, the medium was replaced with 100 mL of DMSO, and the absorbance (570 nm) was measured with an absorbance reader (Thermo Scientific, Multiskan FC). The half-maximal inhibitory concentration (IC_{50}) was determined as the drug concentration leading to 50% inhibition of cell growth.

2.7. Cellular Uptake of the Microcontainers. *2.7.1. Confocal Microscopy.* The cellular uptake and localization was observed using a confocal laser microscope (Leica TCS SP). Cells in the monolayer culture or MTSs were incubated with NR-loaded microcontainers resuspended in serum-free DMEM (0.25 μL of MC per mL) in a 5% CO_2 humidified atmosphere at 37 °C. To visualize nuclei and cytoplasm, the cells were stained with Hoechst solution (50 μM, 10 min) and Calcein AM solution, respectively. In some experiments, in order to inhibit active cell metabolic processes, the cells were incubated with NR-loaded MCs at 4 °C, or a cell membrane was visualized with an another dye, namely, DiO (50 μM, 15 min of incubation in serum-free DMEM). The rest of the manipulations were as described above. Finally, the cells were washed three times with PBS (pH 7.4), mounted in a CC/Mount fluorophor protector, and observed with a Leica confocal microscope. Excitation wavelength values were 360, 488, and 543 nm for Hoechst, DiO, and NR, respectively, while fluorescence signals were collected at 380−460, 500−530 and 560−650 nm for Hoechst, Calcein AM, and NR, respectively. The images were processed in ImageJ software.

2.7.2. Flow Cytometry. For flow cytometry analysis, a BD FACSCalibur fluorescent-activated flow cytometer and BD CellQuest software were used. To prepare samples, NR-loaded MCs resuspended in serum-free DMEM (0.25 μL of MC suspension per mL of medium) were added to the monolayer culture and placed to the CO_2-incubator for 5 and 30 min and 2 h. To remove the MCs that were not

DOI: 10.1021/acsami.5b04141
ACS Appl. Mater. Interfaces 2015, 7, 16581−16589

internalized by cells, the plates were washed three times with PBS (pH 7.4), and then the cells were detached from the plate bottom by trypsinization. After centrifugation (125*g*, 5 min), the cells were resuspended in a 0.4% (w/v) Trypan Blue solution in Hank's balanced salt solution (HBSS) to quench extracellular fluorescence,[20] thus enabling further observation of those MCs that were actually internalized. Finally, the treated samples were subsequently washed twice with PBS (pH 7.4) and analyzed by flow cytometry with at least 10 000 cells being measured in each sample. Fluorescence intensity was quantified in relation to the background fluorescence of nontreated cells.

2.7.3. Fluorimetry. To quantify the MC accumulation inside the tumor spheroids, the NR-loaded MCs resuspended in DMEM (0.25 μL of MC suspension per mL of medium) were added to the MTSs in the plates, and the plates were transferred to the CO_2-incubator for 30 min and 2, 4, 8, and 24 h. Then the MTS were washed with PBS (pH 7.4) and treated with DMSO, and fluorescence was measured using a Promega GloMax-Multi detection system at 525 nm for excitation and 580−640 nm for emission. Uptake data were expressed as a percentage of fluorescence associated with the cells versus fluorescence of the feed solution.

3. RESULTS AND DISCUSSION

3.1. Preparation and Characterization of Microcontainers. In this study, chitosan and xanthan gum have been selected for fabrication of the MCs loaded with lipophilic drug. Chitosan is widely used for production of drug delivery vehicles due to its unique characteristics. First of all, chitosan active primary amino groups are available for chemical modification. Second, chitosan mucoadhesion properties facilitate penetration of chitosan-based particles and conjugates across mucosal and dermal barriers.[21,22] Xanthan gum is also widely employed in food, pharmaceutical, and cosmetic industries due to its mechanical and stabilizing properties.[10]

Here, thymoquinone, which exhibits anti-inflammatory and anticancer effects, was chosen as a model lipophilic drug. Thus, TQ was encapsulated in biodegradable PLGA nanoparticles,[23,24] chitosan nanoparticles,[25] PHA-mPEG copolymer nanocontainers,[26] liposomes,[27] self-assembled cyclodextrin nanoparticles,[28] and solid lipid nanoparticles (SLNs).[29,30] In the current research, TQ was dissolved in soybean oil and loaded to CS/XG microcontainers by ultrasonication. This technique is based on an acoustic cavitation arising during the ultrasonication and inducing production of highly reactive free radicals, mainly $OH^{\bullet}$ and $H^{\bullet}$. The radicals react with polymer moieties located at the interface between the dispersed phase and the dispersion medium, leading to cross-linking and formation of a stable structure. As a result, the oil phase spontaneously emulsifies in the polymer water phase with formation of a cross-linked polymer shell on an emulsion droplet surface. The mechanism of the microcontainers' formation has been described in detail earlier.[8] As shown in Table 1, two TQ-loaded MC fractions with a mean diameter of 0.5 μm (TQ-MC-0.5) and 2 μm (TQ-MC-2) were obtained by varying the oil/water ratio (1:150 and 1:30, respectively). The TQ solubility in soybean oil was up to 400 mg/mL. The TQ content in the soybean oil was found to influence the MC diameter and surface charge only in a minor way. Thus, the ζ-potential value of the TQ-loaded MCs slightly increased without distinct size variability. Modification of the MC surface by PLL polycation adsorption resulted in the surface charge changing, namely, a negative charge rather than a positive one.

Table 1. Mean Size and ζ-Potential Values of the Microcontainers as a Function of Oil/Water Ratio

sample	oil/water ratio	size, nm	ζ-potential, mV
MC-0.5	1/150	512 ± 80	−55
TQ-MC-0.5		530 ± 50	−50
PLL-TQ-MC-0.5		520 ± 80	+20
MC-2	1/30	2051 ± 200	−52
TQ-MC-2		1952 ± 250	−48
PLL-TQ-MC-2		2130 ± 150	+20

Cryo-SEM images of the MC-0.5 and MC-2 fractions are shown in Figure 1. The core−shell structure of the MCs (Figure 1C) was described in detail earlier.[8] MCs did not aggregate in water solutions, which could be explained by rather high negative surface charge, which is a key factor to stabilize colloidal dispersions. However, the negative surface charge could make the accumulation of MCs in tumor cells difficult. Thus, as well-known, tumor cells have a bigger negative surface charge compared to normal cells due to sialic acid expression[31] and the abundance of heparin sulfate.[32] Moreover, tight junctions between epithelial cells and cells of stratium corneum in the skin are also negatively charged.[21] So, we supposed that the positively charged MCs could be preferable for adhesion on the skin cells. The MC surface was modified with PLL by electrostatic adsorption. PLL is commonly used for modification of DNA/RNA carriers,[33] including particles for targeted delivery.[34] The TQ-loaded MCs demonstrated rather good stability in complete culture medium (DMEM +10% FBS). After 24 h incubation of the MCs in the medium, the mean MC-0.5 size increased from 512 ± 80 to 552 ± 50 nm, while the ζ-potential changed from −55 to −48 mV. This could be explained by adsorption of serum proteins on the MC surface.

3.2. Accumulation of the Microcontainers in a Monolayer Culture. Cellular uptake and intracellular localization of the MCs were assessed using mouse melanoma M-3 cells by confocal microscopy and flow cytometry (Figure 2). To visualize the microcontainers, a NR lipophilic dye was entrapped in the MC oil core. As seen in Figure 2A,D, both the MC-0.5 and MC-2 samples were found in cell membranes,-even after 5 min incubation. A significant enhancement of the MC accumulation was observed in 30 min and 2 h (Figure 2B,C,E,F). However, the MC-0.5 and MC-2 accumulation within the cells differed. Thus, after 2 h incubation, the fluorescence intensity of the MC-0.5 sample was 2-fold higher than that of the MC-2 fraction (Figure 2G). Most of the MCs were found to be localized in the cell membrane, and an obvious engulfment of the MCs in a cytosol was observed only after 2 h incubation (Figure 2F, see an inset). The MCs maintained stablity in the cytoplasm at least for 2 h, which was confirmed by their dotlike fluorescence.

We could suggest that rather rapid accumulation on cell membranes and subsequent rather slow penetration of the MCs into the cytoplasm could be explained by a two-stage mechanism of this process. At the first stage, MC adsorption occurred at the cell surface due to rather strong electrostatic interactions. At the second stage, the MCs could be transferred from the cell membranes to the cytosol in a time- and energy-dependent manner. To verify this hypothesis, the MCs were incubated with the cells at low temperature (4 °C), which inhibited all cellular activities, including endocytosis. As seen in Figure 3A,B, at 4 °C the NR-loaded MC-0.5 were obviously colocalized with the membranes marked with DiO lipophilic dye but not with the cytoplasm, which was stained with Calcein AM. Since we did not observe the engulfed MCs in the

DOI: 10.1021/acsami.5b04141
ACS Appl. Mater. Interfaces 2015, 7, 16581−16589

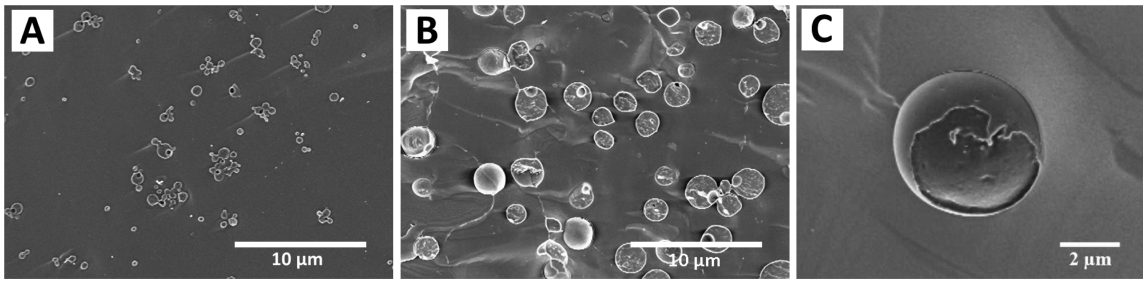

Figure 1. Cryo-SEM images of the MC-0.5 (A) and MC-2 (B) particles and a container with a broken shell (C).

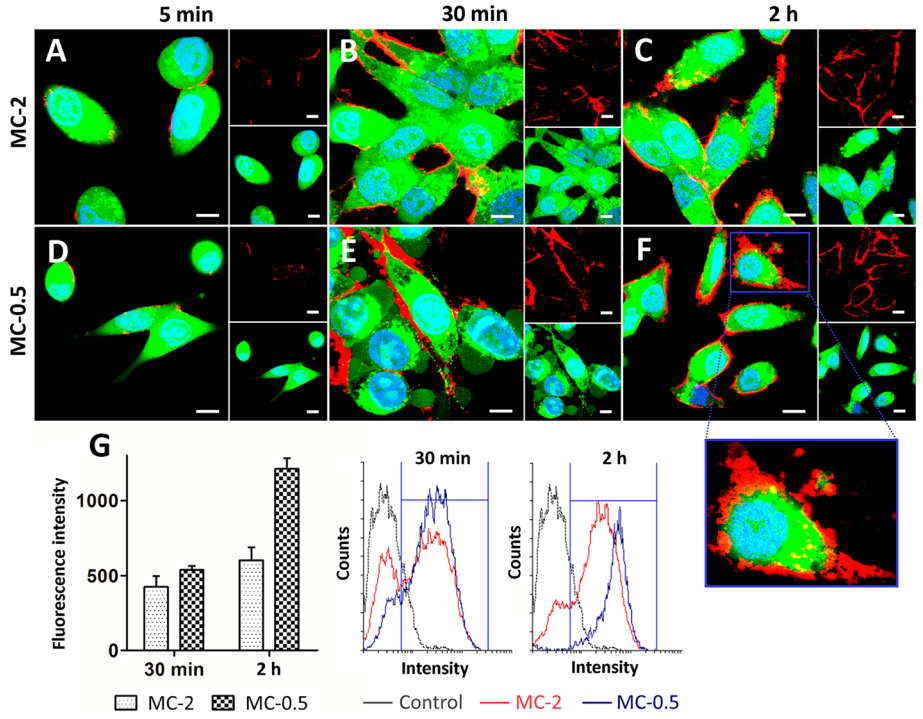

Figure 2. Uptake of the Nile Red-loaded microcontainers (MC-0.5 and MC-2) by mouse melanoma M-3 cells in 5 and 30 min and 2 h: confocal microscopy images (A–F) and flow cytometry data (G). Cell nuclei and cytoplasm were stained with Hoechst (in blue) and Calcein AM (in green), respectively. Insets on the upper right show the NR signal distributed in the MCs, insets on the bottom right show cell and nucleus signals, while larger pictures on the left show both signals merged. The scale- bar is 10 μm. Flow cytometry data are expressed as median fluorescent intensity divided by the background intensity of control (nontreated cells) after 30 min and 2 h incubation with MCs (2.5 μL of MC suspension per mL of medium). A right shift of the intensity curves indicates the MC accumulation in the cells.

cytoplasm after 2 h incubation at 4 °C, we supposed that the energy-dependent path occurred. The observed two-stage process is in good agreement with previously reported internalization pathways of polyelectrolyte multilayer capsules into mammalian cells.[35] The above mentioned two-step mechanism allows one to rapidly incorporate rather large amounts of an active agent directly into cellular membrane with the following prolonged MC transportation into the cells.

Modification of nanoparticles with PLL was found to enhance intracellular delivery.[36] As was expected, in our case modification of the MC surface with PLL resulted in the double MC accumulation increase within the cells after 2 h incubation (Figure 3 C).

3.3. Accumulation of the Microcontainers in Multicellular Tumor Spheroids. For the past 30 years, 2D cell-based assay models have dominated preclinical cancer drug discovery efforts. 2D cell-based models fail to predict in vivo efficacy, contributing to a lower success rate and higher cost required to translate an investigational new drug to clinical approval. Technological advances in 3D cell culture models bridge the gap between 2D and in vivo models to improve upon the current success rates for cancer drug discovery. Multicellular tumor spheroids are considered as a promising 3D in vitro model in tumor biology.[37] The main advantages of MTSs as a 3D growth system are their chemically and spatially defined 3D network of extracellular matrix components, cell-to-cell and cell-to-matrix interactions which govern differentiation, proliferation, and cell function in vivo.[38,39] All of these factors can hinder efficacy of both drug and drug nanocarriers either by mass transport limitations or by promoting drug resistance.[40] Recently, we used microencapsulated MTS as a tool to test novel anticancer nanosized drug delivery systems in vitro[41] and to study the effects of photodynamic therapy.[42] In the current study, we are focused on evaluation of the MC penetration and accumulation within tumor spheroids. Generally, a penetration of drug-loaded vehicles into solid tumors is limited, since they have to pass through several cellular layers, such as smooth muscle cells and fibroblasts, before they reach tumor cells.

DOI: 10.1021/acsami.5b04141
ACS Appl. Mater. Interfaces 2015, 7, 16581–16589

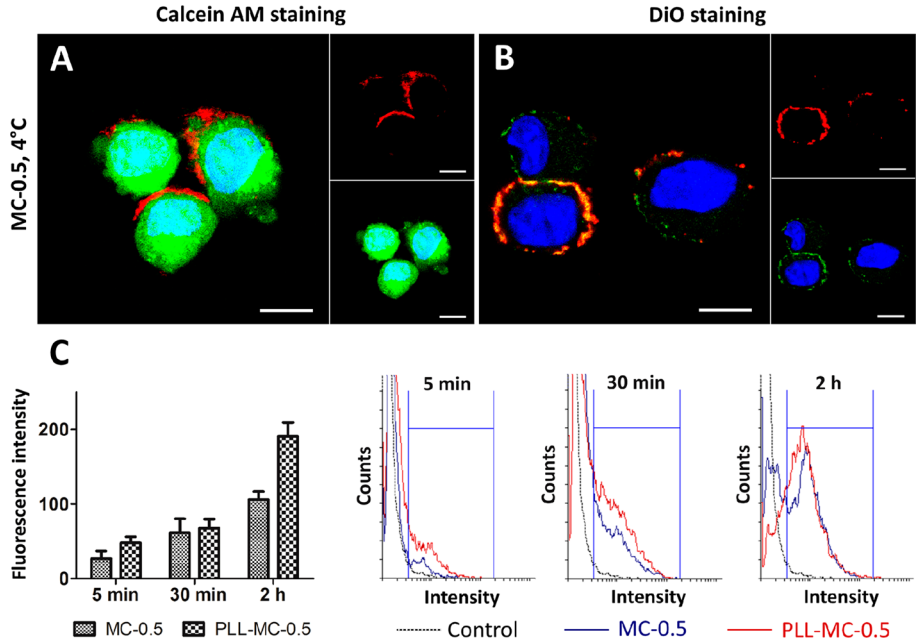

Figure 3. Uptake of the Nile Red-loaded MC-0.5 and PLL-MC-0.5 by M3 cells: confocal microscopy images (A, B) and flow cytometry data (C). For confocal microscopy, the cells were incubated with NR-loaded MC-0.5 for 2 h at 4 °C. The cells were stained with Hoechst (cell nuclei, in blue) and Calcein AM (cytoplasm, in green) in image A and with DiO (cell membrane, in green) in image B. Insets on the upper right show the NR signal in the MCs, and insets on the bottom right show cell and nuclei signals, while larger pictures on the left show both signals merged. The scale bar is 10 μm. Flow cytometry data are expressed as median fluorescent intensity divided by the background intensity of control (nontreated cells) after 5 and 30 min and 2 h incubation (0.25 μL of MC suspension per mL of medium). A right shift of intensity curves indicates the MC localization within the cells.

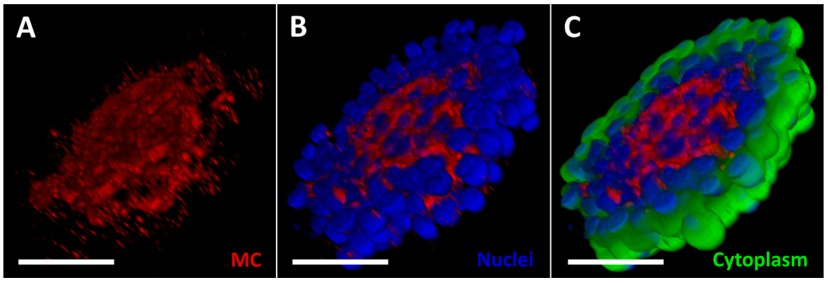

Figure 4. Confocal images of a tumor spheroid cross section after 4 h incubation with NR-loaded MC-0.5 particles. The images were obtained with 3D Viewer plugin (ImageJ software) from a series of stepwise confocal snapshots (one step was about 1 μm). MCs were loaded with Nile Red (A–C, in red), cell nuclei were stained with Hoechst (B–C, in blue), and cytoplasm of alive cells was stained with Calcein AM (C, in green). The scale bar is 50 μm.

Consequently, rather high cell density in tumors makes the penetration of drug delivery systems difficult, since they are able to infiltrate only three to five cell diameters into the tumor.[43] To evaluate the MC penetration ability, tumor spheroids (120–180 μm) were generated from M-3 cells by a novel, highly reproducible technique recently developed in our lab.[53] Accumulation of MC-0.5 microcontainers within the tumor spheroid is shown in Figure 4. As can be seen, the cells in spheroids were arranged in a compact, dense structure and were alive, which was revealed using Calcein AM staining. No necrotic core was found in the center of spheroids. This is in good agreement with the knowledge that a necrotic core appears in spheroids that are larger than 400–500 μm in diameter.[44,45]

Both MC-0.5 and MC-2 samples were found to penetrate into the spheroids in a time-dependent manner, but the penetration depth was different. Thus, MC-0.5 were observed in the spheroid outer layer after 1 h incubation, while after 4 h they reached already the cells in the spheroid center (Figure 5A,B). As for MC-2 sample, the penetration depth was smaller compared to that of MC-0.5, especially after 4 h (Figure 5D,E). Moreover, fluorescence levels of the MC-0.5 sample were doubly higher compared to that of the MC-2 sample after 8 and 24 h incubation (Figure 5F). This observation confirmed the idea that MC-0.5 particles could be more promising for drug delivery. The MC localization in the spheroids was similar to that previously observed for monolayer culture (see Figure 2); namely, the MCs were mostly found in the cell membrane (Figure 5C).

3.4. Cytotoxicity Study. Melanoma is considered as the most dangerous form of skin cancer, causing 90% mortality.[46] Recently, the TQ antitumor effect against human and mouse melanoma cells in vitro as well as the TQ ability to inhibit metastasis in a mouse melanoma model were reported.[47] It should be noted that the TQ antitumor effect could be related to multiple mechanisms. For instance, TQ was found to induce

DOI: 10.1021/acsami.5b04141
ACS Appl. Mater. Interfaces 2015, 7, 16581–16589

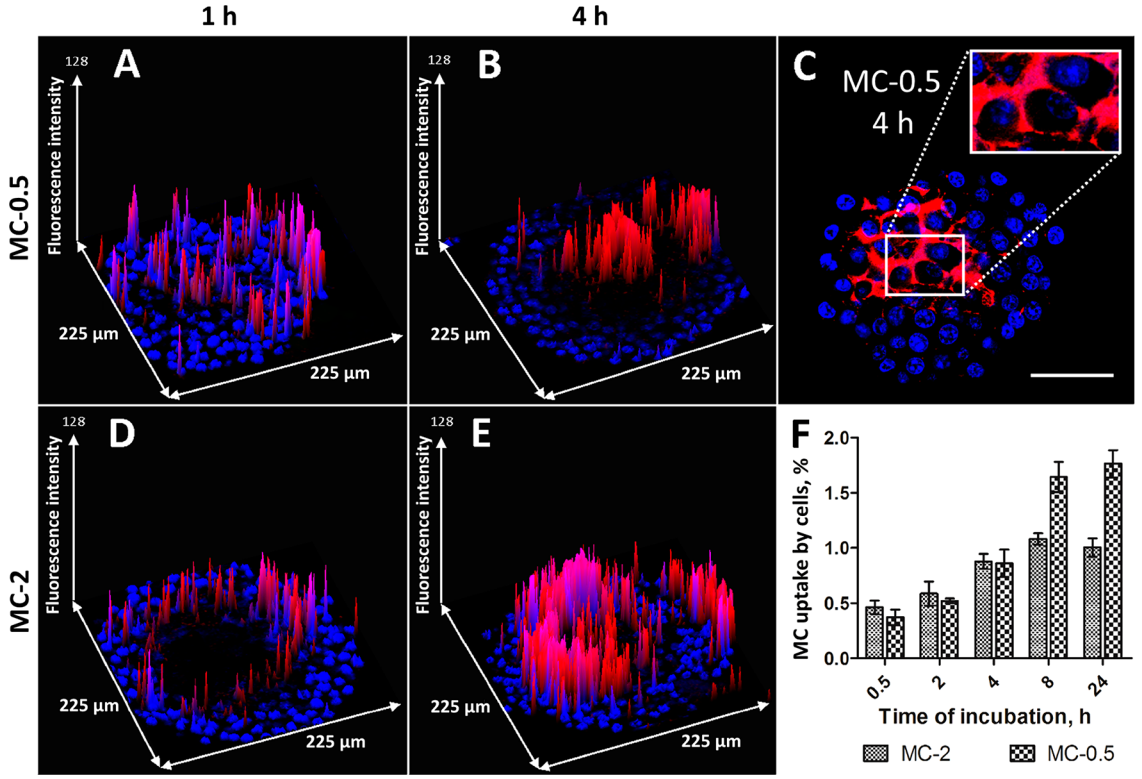

Figure 5. Distribution (A–E) and accumulation (F) of the NR-loaded microcontainers in M-3 cells-based tumor spheroids: surface plots of the spheroids treated with MC-0.5 (A–C) and MC-2 (D, E) samples after 1 and 4 h of incubation and fluorimetry data of uptake of the MCs by the cells in the spheroids (F). Cell nuclei were stained with Hoechst (in blue). Fluorimetry data are expressed as percent of fluorescent intensity compared to that of the MCs in feed suspension.

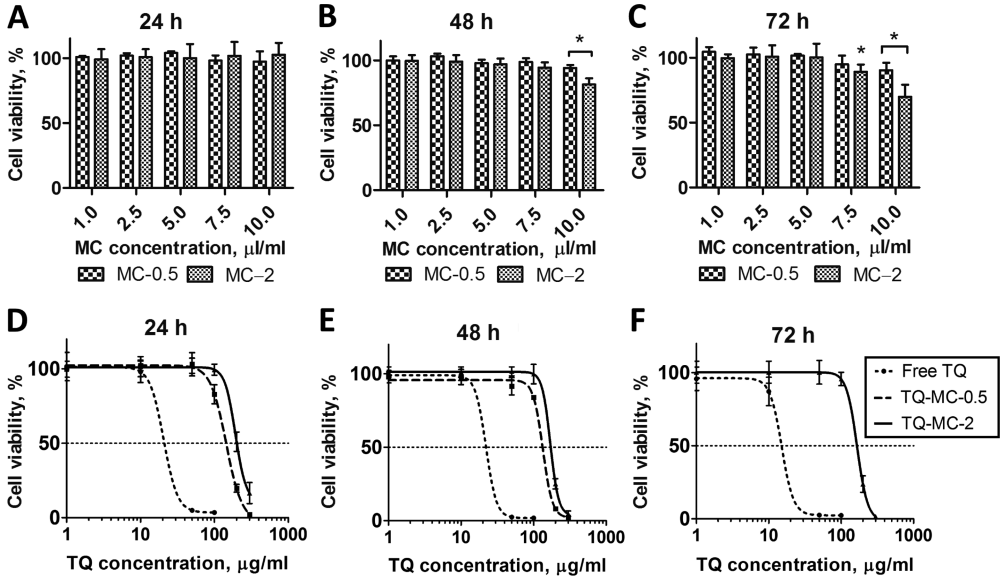

Figure 6. Viability of M-3 cells after incubation with blank MCs (A–C) and TQ-loaded MCs (D–F). MTT assay data. The control (nontreated cells) was taken as 100%. Values are means ± SD of three independent experiments; two-tailed *P*-values were calculated by the unpaired *t* test (* indicates a *P*-value <0.05).

generation of a reactive oxygen species[48,49] and to decrease glutathione levels in a dose-dependent manner.[50] Moreover, TQ has been also shown to inhibit telomerase and to induce telomere shortening and apoptosis in glioblastoma cell lines.[51] Finally, it inhibits microtubule polymerization by tubulin binding and causes mitotic arrest following apoptosis in nonsmall cell lung carcinoma A549 cells.[52] Here, to study the cytotoxicity of the TQ-loaded microcontainers, murine melanoma M-3 cells were used. First, we evaluated the cytotoxicity of the blank MCs as a function of the MC size (Figure 6A–C). The use of MC-0.5 did not cause any cell death until a concentration of 10 μL of the MC suspension per 1 mL of DMEM. As for the MC-2 sample, we revealed rather weak but statistically significant cytotoxicity of these micro-

DOI: 10.1021/acsami.5b04141
ACS Appl. Mater. Interfaces 2015, 7, 16581–16589

containers at a concentration of 7.5 μL per mL of DMEM after 48 and 72 h incubation. The higher cytotoxicity of the MC-2 sample compared to that of the MC-0.5 particles most probably could be related to the greater oil content in each MC-2 bead than in each MC-0.5 particle.

As seen in Figure 6E,F, the TQ-loaded MCs were able to inhibit melanoma cell growth. The cytotoxicity was found to depend upon of the MC size and incubation time. Thus, in the case of TQ-MC-2, the IC_{50} values were 193.0 ± 2.0, 170.1 ± 1.7, and 166.0 ± 2.3 μg/mL after 24, 48, and 72 h incubation, respectively, while for TQ-MC-0.5 the IC_{50} values were lower, namely, 144.9 ± 1.4 and 134.1 ± 1.1 μg/mL in 24 and 48 h, respectively (Figure 6E,F). The higher cytotoxicity of the TQ-MC-0.5 fraction compared to the TQ-MC-2 sample is in good correlation with the better accumulation of the MC-0.5 in the cells. As seen in Figure 4D, the anticancer effect of free TQ was higher compared to that of the drug loaded in the MC. In particular, IC_{50} values of free TQ were 22.1 ± 1.4, 20.7 ± 1.5, and 15.2 ± 1.1 μg/mL in 24, 48, and 72 h. A lower efficacy of the TQ-loaded MCs compared to that of the free drug could be explained by the time-dependent TQ release from the microcontainers.

4. CONCLUSIONS

The ultrasound-induced chitosan−xanthan gum microcontainers were fabricated and characterized in terms of their size and ζ-potential. Accumulation of two MC fractions with a mean size of 500 nm (MC-0.5) and 2 μM (MC-2) loaded with Nile Red dye into mouse melanoma M-3 cells was evaluated by confocal microscopy, flow cytometry, and fluorimetry. Modification of the MCs with PLL allowed one to get double the MC accumulation within the cells. The MC were loaded with thymoquinone, and their cytotoxicity was tested. The MC-0.5 particles were more promising as drug delivery systems than MC-2 beads because of their higher cellular uptake both in 2D and 3D models, an enhanced antitumor effect, and a lower level of nonspecific toxicity.

AUTHOR INFORMATION

Corresponding Author

*E-mail: roman.akasov@gmail.com.

Notes

The authors declare no competing financial interest.

ACKNOWLEDGMENTS

The study was partially supported by RFBR (project No. 12-04-31687 mol_a). This work was performed using the equipment of the Shared Research Center IC RAS and supported by the Ministry of Education and Science of the Russian Federation.

ABBREVIATIONS USED

CS = chitosan
XG = xanthan gum
MC = microcontainers
MTS = multicellular tumor spheroids
NR = Nile Red
TQ = thymoquinone
PLL = poly-L-lysine

REFERENCES

(1) Rowinsky, E. K. The Development and Clinical Utility of the Taxane Class of Antimicrotubule Chemotherapy Agents. *Annu. Rev. Med.* **1997**, *48*, 353−374.
(2) Hoy, S. M. Albumin-Bound Paclitaxel: A Review of Its Use for the First-Line Combination Treatment of Metastatic Pancreatic Cancer. *Drugs* **2014**, *74*, 1757−1768.
(3) Ma, P.; Mumper, R. J. Paclitaxel Nano-Delivery Systems: A Comprehensive Review. *J. Nanomed. Nanotechnol.* **2013**, *4*, 1000164.
(4) Wu, J.; Zhu, Y. J.; Cao, S. W.; Chen, F. Hierachically Nanostructured Mesoporous Spheres of Calcium Silicate Hydrate: Surfactant-Free Sonochemical Synthesis and Drug-Delivery System with Ultrahigh Drug-Loading Capacity. *Adv. Mater. (Weinheim, Ger.)* **2010**, *22*, 749−753.
(5) Grinstaff, M. W.; Suslick, K. S. Air-Filled Proteinaceous Microbubbles: Synthesis of an Echo-Contrast Agent. *Proc. Natl. Acad. Sci. U. S. A.* **1991**, *88*, 7708−7710.
(6) Silva, R.; Ferreira, H.; Cavaco-Paulo, A. Sonoproduction of Liposomes and Protein Particles as Templates for Delivery Purposes. *Biomacromolecules* **2011**, *12*, 3353−3368.
(7) Bang, J. H.; Suslick, K. S. Applications of Ultrasound to the Synthesis of Nanostructured Materials. *Adv. Mater. (Weinheim, Ger.)* **2010**, *22*, 1039−1059.
(8) Borodina, T. N.; Grigoriev, D. O.; Carillo, M. a.; Hartmann, J.; Moehwald, H.; Shchukin, D. G. Preparation of Multifunctional Polysaccharide Microcontainers for Lipophilic Bioactive Agents. *ACS Appl. Mater. Interfaces* **2014**, *6*, 6570−6578.
(9) Wang, J. J.; Zeng, Z. W.; Xiao, R. Z.; Xie, T.; Zhou, G. L.; Zhan, X. R.; Wang, S. L. Recent Advances of Chitosan Nanoparticles as Drug Carriers. *Int. J. Nanomed.* **2011**, *6*, 765−774.
(10) Badwaik, H. R.; Giri, T. K.; Nakhate, K. T.; Kashyap, P.; Tripathi, D. K. Xanthan Gum and Its Derivatives as a Potential Bio-Polymeric Carrier for Drug Delivery System. *Curr. Drug Delivery* **2013**, *10*, 587−600.
(11) Hafner, A.; Lovrić, J.; Pepić, I.; Filipović-Grčić, J. Lecithin/chitosan Nanoparticles for Transdermal Delivery of Melatonin. *J. Microencapsulation* **2011**, *28*, 807−815.
(12) Kim, J. H.; Kim, Y. S.; Park, K.; Kang, E.; Lee, S.; Nam, H. Y.; Kim, K.; Park, J. H.; Chi, D. Y.; Park, R. W.; Kim, I. S.; Choi, K.; Chan Kwon, I. Self-Assembled Glycol Chitosan Nanoparticles for the Sustained and Prolonged Delivery of Antiangiogenic Small Peptide Drugs in Cancer Therapy. *Biomaterials* **2008**, *29*, 1920−1930.
(13) Caddeo, C.; Nácher, a; Diez-Sales, O.; Merino-Sanjuán, M.; Fadda, a M.; Manconi, M. Chitosan-Xanthan Gum Microparticle-Based Oral Tablet for Colon-Targeted and Sustained Delivery of Quercetin. *J. Microencapsulation* **2014**, *31*, 694−699.
(14) Ferreira, D. M.; Saga, Y. Y.; Aluicio-Sarduy, E.; Tedesco, A. C. Chitosan Nanoparticles for Melanoma Cancer Treatment by Photodynamic Therapy and Electrochemotherapy Using Aminolevulinic Acid Derivatives. *Curr. Med. Chem.* **2013**, *20*, 1904−1911.
(15) Battogtokh, G.; Ko, Y. T. Self-Assembled Polymeric Nanoparticle of PEGylated Chitosan−ceramide Conjugate for Systemic Delivery of Paclitaxel. *J. Drug Targeting* **2014**, *22*, 813−821.
(16) Banerjee, S.; Kaseb, A. O.; Wang, Z.; Kong, D.; Mohammad, M.; Padhye, S.; Sarkar, F. H.; Mohammad, R. M. Antitumor Activity of Gemcitabine and Oxaliplatin Is Augmented by Thymoquinone in Pancreatic Cancer. *Cancer Res.* **2009**, *69*, 5575−5583.
(17) Racoma, I. O.; Meisen, W. H.; Wang, Q.-E.; Kaur, B.; Wani, A. A. Thymoquinone Inhibits Autophagy and Induces Cathepsin-Mediated, Caspase-Independent Cell Death in Glioblastoma Cells. *PLoS One* **2013**, *8*, e72882.
(18) Salmani, J. M. M.; Asghar, S.; Lv, H.; Zhou, J. Aqueous Solubility and Degradation Kinetics of the Phytochemical Anticancer Thymoquinone; Probing the Effects of Solvents, pH and Light. *Molecules* **2014**, *19*, 5925−5939.
(19) Schneider-Stock, R.; Fakhoury, I. H.; Zaki, A. M.; El-Baba, C. O.; Gali-Muhtasib, H. U. Thymoquinone: Fifty Years of Success in the Battle against Cancer Models. *Drug Discovery Today* **2014**, *19*, 18−30.

DOI: 10.1021/acsami.5b04141
ACS Appl. Mater. Interfaces 2015, 7, 16581−16589

(20) Van Amersfoort, E. S.; Van Strijp, J. A. G. Evaluation of a Flow Cytometric Fluorescence Quenching Assay of Phagocytosis of Sensitized Sheep Erythrocytes by Polymorphonuclear Leukocytes. *Cytometry* **1994**, *17*, 294−301.
(21) Chen, Y.; Wang, M.; Fang, L. Biomaterials as Novel Penetration Enhancers for Transdermal and Dermal Drug Delivery Systems. *Drug Delivery* **2013**, *20*, 199−209.
(22) Hu, L.; Sun, Y.; Wu, Y. Advances in Chitosan-Based Drug Delivery Vehicles. *Nanoscale* **2013**, *5*, 3103−3111.
(23) Ganea, G. M.; Fakayode, S. O.; Losso, J. N.; van Nostrum, C. F.; Sabliov, C. M.; Warner, I. M. Delivery of Phytochemical Thymoquinone Using Molecular Micelle Modified poly(D, L Lactide-Co-Glycolide) (PLGA) Nanoparticles. *Nanotechnology* **2010**, *21*, 285104.
(24) Ravindran, J.; Nair, H. B.; Sung, B.; Prasad, S.; Tekmal, R. R.; Aggarwal, B. B. Thymoquinone Poly(lactide-co-glycolide) Nanoparticles Exhibit Enhanced Anti-Proliferative, Anti-Inflammatory, and Chemosensitization Potential. *Biochem. Pharmacol. (Amsterdam, Neth.)* **2010**, *79*, 1640−1647.
(25) Alam, S.; Khan, Z. I.; Mustafa, G.; Kumar, M.; Islam, F.; Bhatnagar, A.; Ahmad, F. J. Development and Evaluation of Thymoquinone-Encapsulated Chitosan Nanoparticles for Nose-to-Brain Targeting: A Pharmacoscintigraphic Study. *Int. J. Nanomed.* **2012**, *7*, 5705−5718.
(26) Shah, M.; Naseer, M. I.; Choi, M. H.; Kim, M. O.; Yoon, S. C. Amphiphilic PHA-mPEG Copolymeric Nanocontainers for Drug Delivery: Preparation, Characterization and in Vitro Evaluation. *Int. J. Pharm. (Amsterdam, Neth.)* **2010**, *400*, 165−175.
(27) Odeh, F.; Ismail, S. I.; Abu-Dahab, R.; Mahmoud, I. S.; Al Bawab, A. Thymoquinone in Liposomes: A Study of Loading Efficiency and Biological Activity towards Breast Cancer. *Drug Delivery* **2012**, *19*, 371−377.
(28) Abu-Dahab, R.; Odeh, F.; Ismail, S. I.; Azzam, H.; Al Bawab, A. Preparation, Characterization and Antiproliferative Activity of Thymoquinone-B-Cyclodextrin Self Assembling Nanoparticles. *Int. J. Pharm. Pharm. Sci.* **2013**, *68*, 939−944.
(29) Pathan, S. a.; Jain, G. K.; Zaidi, S. M. a; Akhter, S.; Vohora, D.; Chander, P.; Kole, P. L.; Ahmad, F. J.; Khar, R. K. Stability-Indicating Ultra-Performance Liquid Chromatography Method for the Estimation of Thymoquinone and Its Application in Biopharmaceutical Studies. *Biomed. Chromatogr.* **2011**, *25*, 613−620.
(30) Singh, A.; Ahmad, I.; Akhter, S.; Jain, G. K.; Iqbal, Z.; Talegaonkar, S.; Ahmad, F. J. Nanocarrier Based Formulation of Thymoquinone Improves Oral Delivery: Stability Assessment, in Vitro and in Vivo Studies. *Colloids Surf., B* **2013**, *102*, 822−832.
(31) Márquez, M.; Nilsson, S.; Lennartsson, L.; Liu, Z.; Tammela, T.; Raitanen, M.; Holmberg, A. R. Charge-Dependent Targeting: Results in Six Tumor Cell Lines. *Anticancer Res.* **2004**, *24*, 1347−1352.
(32) Ang, I. L.; Poon, T. C. W.; Lai, P. B. S.; Chan, A. T. C.; Ngai, S.; Hui, A. Y.; Johnson, P. J.; Sung, J. J. Y. Study of Serum Haptoglobin and Its Glycoforms in the Diagnosis of Hepatocellular Carcinoma; A Glycoproteomic Approach; Ang, IL; Journal of Proteome Research 2006, 5, 2691−2700.pdf. *J. Proteome Res.* **2006**, *5*, 2691−2700.
(33) Du, J.; Sun, Y.; Shi, Q. S.; Liu, P. F.; Zhu, M. J.; Wang, C. H.; Du, L. F.; Duan, Y. R. Biodegradable Nanoparticles of mPEG-PLGA-PLL Triblock Copolymers as Novel Non-Viral Vectors for Improving siRNA Delivery and Gene Silencing. *Int. J. Mol. Sci.* **2012**, *13*, 516−533.
(34) Tian, H.; Lin, L.; Jiao, Z.; Guo, Z.; Chen, J.; Gao, S.; Zhu, X.; Chen, X. Polylysine-Modi Fi Ed Polyethylenimine Inducing Tumor Apoptosis as an Ef Fi Cient Gene Carrier. *J. Controlled Release* **2013**, *172*, 410−418.
(35) Kastl, L.; Sasse, D.; Wulf, V.; Hartmann, R.; Mircheski, J.; Ranke, C.; Carregal-Romero, S.; Martínez-López, J. A.; Fernández-Chacón, R.; Parak, W. J.; Elsasser, H. P.; Rivera Gil, P. Multiple Internalization Pathways of Polyelectrolyte Multilayer Capsules into Mammalian Cells. *ACS Nano* **2013**, *7*, 6605−6618.
(36) Deshpande, S.; Venugopal, E.; Ramagiri, S.; Bellare, J. R.; Kumaraswamy, G.; Singh, N. Enhancing Cubosome Functionality by Coating with a Single Layer of Poly-E-Lysine. *ACS Appl. Mater. Interfaces* **2014**, *6*, 17126−17133.
(37) LaBarbera, D. V.; Reid, B. G.; Yoo, B. H. The Multicellular Tumor Spheroid Model for High-Throughput Cancer Drug Discovery. *Expert Opin. Drug Discovery* **2012**, *7*, 819−830.
(38) Hickman, J. a; Graeser, R.; de Hoogt, R.; Vidic, S.; Brito, C.; Gutekunst, M.; van der Kuip, H. Three-Dimensional Models of Cancer for Pharmacology and Cancer Cell Biology: Capturing Tumor Complexity in Vitro/ex Vivo. *Biotechnol. J.* **2014**, *9*, 1115−1128.
(39) Xu, X.; Farach-Carson, M. C.; Jia, X. Three-Dimensional in Vitro Tumor Models for Cancer Research and Drug Evaluation. *Biotechnol. Adv.* **2014**, *32*, 1256−1268.
(40) Sagnella, S.; Duong, H.; MacMillan, A.; Boyer, C.; Whan, R.; McCarroll, J. A.; Davis, T.P.; Kavallaris, M. Dextran Based Doxorubicin Nanocarriers with Improved Tumour Penetration. *Biomacromolecules* **2013**, *15*, 262−275.
(41) Privalova, A. M.; Uglanova, S. V.; Kuznetsova, N. R.; Klyachko, N. L.; Golovin, Y. I.; Korenkov, V. V.; Vodovozova, E. L.; Markvicheva, E. A. Microencapsulated Multicellular Tumor Spheroids as a Tool to Test Novel Anticancer Nanosized Drug Delivery Systems In Vitro. *J. Nanosci. Nanotechnol.* **2015**, *15*, 4806−4814.
(42) Zaytseva-Zotova, D. S.; Udartseva, O. O.; Andreeva, E. R.; Bartkowiak, A.; Bezdetnaya, L. N.; Guillemin, F.; Goergen, J. L.; Markvicheva, E. a. Polyelectrolyte Microcapsules with Entrapped Multicellular Tumor Spheroids as a Novel Tool to Study the Effects of Photodynamic Therapy. *J. Biomed. Mater. Res., Part B* **2011**, *97B*, 255−262.
(43) Lammers, T.; Kiessling, F.; Hennink, W. E.; Storm, G. Drug Targeting to Tumors: Principles, Pitfalls and (Pre-) Clinical Progress. *J. Controlled Release* **2012**, *161*, 175−187.
(44) Mehta, G.; Hsiao, A. Y.; Ingram, M.; Luker, G. D.; Takayama, S. Opportunities and Challenges for Use of Tumor Spheroids as Models to Test Drug Delivery and Efficacy. *J. Controlled Release* **2012**, *164*, 192−204.
(45) Neto, a. I.; Correia, C. R.; Oliveira, M. B.; Rial-Hermida, M. I.; Alvarez-Lorenzo, C.; Reis, R. L.; Mano, J. F. A Novel Hanging Spherical Drop System for the Generation of Cellular Spheroids and High Throughput Combinatorial Drug Screening. *Biomater. Sci.* **2015**, *3*, 581−585.
(46) Garbe, C.; Peris, K.; Hauschild, A.; Saiag, P.; Middleton, M.; Spatz, A.; Grob, J. J.; Malvehy, J.; Newton-Bishop, J.; Stratigos, A.; Pehamberger, H.; Eggermont, A. M. Diagnosis and Treatment of Melanoma. European Consensus-Based Interdisciplinary Guideline - Update 2012. *Eur. J. Cancer* **2012**, *48*, 2375−2390.
(47) Ahmad, I.; Muneer, K. M.; Tamimi, I. a.; Chang, M. E.; Ata, M. O.; Yusuf, N. Thymoquinone Suppresses Metastasis of Melanoma Cells by Inhibition of NLRP3 Inflammasome. *Toxicol. Appl. Pharmacol.* **2013**, *270*, 70−76.
(48) Dergarabetian, E. M.; Ghattass, K. I.; El-Sitt, S. B.; Al-Mismar, R. M.; El-Baba, C. O.; Itani, W. S.; Melhem, N. M.; El-Hajj, H. A.; Bazarbachi, A. A. H.; Schneider-Stock, R.; Gali-Muhtasib, H. U. Thymoquinone Induces Apoptosis in Malignant T-Cells via Generation of ROS. *Front. Biosci., Elite Ed.* **2013**, *5*, 706−719.
(49) Gali-Muhtasib, H.; Ocker, M.; Kuester, D.; Krueger, S.; El-Hajj, Z.; Diestel, A.; Evert, M.; El-Najjar, N.; Peters, B.; Jurjus, A.; Roessner, A.; Schneider-Stock, R. Thymoquinone Reduces Mouse Colon Tumor Cell Invasion and Inhibits Tumor Growth in Murine Colon Cancer Models. *J. Cell. Mol. Med.* **2008**, *12*, 330−342.
(50) Rooney, S.; Ryan, M. F. Modes of Action of Alpha-Hederin and Thymoquinone, Active Constituents of Nigella Sativa, against HEp-2 Cancer Cells. *Anticancer Res.* **2005**, *25*, 4255−4259.
(51) Gurung, R. L.; Lim, S. N.; Khaw, A. K.; Soon, J. F. F.; Shenoy, K.; Ali, S. M.; Jayapal, M.; Sethu, S.; Baskar, R.; Prakash Hande, M. Thymoquinone Induces Telomere Shortening, DNA Damage and Apoptosis in Human Glioblastoma Cells. *PLoS One* **2010**, *5*, e12124.
(52) Acharya, B. R.; Chatterjee, A.; Ganguli, A.; Bhattacharya, S.; Chakrabarti, G. Thymoquinone Inhibits Microtubule Polymerization by Tubulin Binding and Causes Mitotic Arrest Following Apoptosis in A549 Cells. *Biochimie* **2014**, *97*, 78−91.

DOI: 10.1021/acsami.5b04141
ACS Appl. Mater. Interfaces 2015, 7, 16581−16589

(53) Akasov, R.; Zaytseva-Zotova, D.; Burov, S.; Leko, M.; Dontenwill, M.; Chiper, M.; Vandamme, T.; Markvicheva, E. Manuscript submitted.

DOI: 10.1021/acsami.5b04141
ACS Appl. Mater. Interfaces 2015, 7, 16581−16589